PCCP

Accepted Manuscript

ROYAL SOCIETY
OF CHEMISTRY

www.rsc.org/pccp

PAPER

Au$_{13-n}$Ag$_n$ Clusters: A Remarkably Simple Trend

Francisco Munoz,[a,b] **Alejandro Varas,**[a,b,c] **José Rogan,**[a,b‡] **Juan Alejandro Valdivia,**[a,b] **and Miguel Kiwi**[*a,b]

The planar to three dimensional transition of Au$_{13-n}$Ag$_n$ clusters is investigated. To do so the low lying energy configurations for all possible concentrations (n values), are evaluated. Many thousand of possible conformations are examined. They are generated using the procedure by Rogan *et al.*[1] in combination with the semi-empirical Gupta potential.[2,3] A large fraction of these (the low lying energy ones) are minimized by means of Density Functional Theory (DFT) calculations. We employ the Tao, Perdew, Staroverov, and Scuseria (TPSS) meta-GGA functional and the Perdew, Burke and Ernzerhof (PBE) GGA functional, and compare their results. The effect of spin-orbit coupling is studied as well as the s-d hybridization. As usual in this context the results are functional-dependent. However, both functionals lead to agreement as far as trends are concerned, yielding just two relevant motifs, but their results differ quantitatively.

1 Introduction

The planar to volumetric (or 2D ↔ 3D) transition of nanoclusters has attracted significant interest for a long time.[4–6] However, during the last few years several authors reexamined the problem to correct and clarify the question using recently developed, and more powerful, techniques.[7–12] The reexamination of this issue derives from the circumstance that for neutral gold clusters there is little experimental information, and theoretical results on the 2D ↔ 3D transition do not agree; and in fact, they are in rather strong disagreement,[8] and seem to depend on the functional that is used.

The interest in small gold clusters is driven by the close interplay between their physical and chemical properties, and the technological implications they have for catalysis,[13] optical activity,[14] and medical applications,[15] among others. The basic properties and potential applications are strongly determined by the 2D or 3D character of the conformation. The problem is also relevant since in nanosystems the s-p-d hybridization, as well as the 5d shell bonding, become important elements in the understanding of the chemistry of pure and alloyed Au clusters. All in all, since bulk Au is a 6s prototype for a quasi-free electron system, the difference between nanocluster and bulk electronic properties is relevant from a basic point of view, and may constitute a key ingredient for

applications at the nanoscopic level.

Once pristine gold nanoclusters were reasonably well investigated the question arose of how alloying, mainly with coinage metals, modifies the pure Au results. Most work has focused on dilute doping of the Au clusters, as done by Dong *et al.*[16] who added a single Mn atom to Au$_N$ clusters, for $1 \le N \le 8$, finding that all the ground states and the low lying excitations are planar, and that Mn atoms in the groundstate of the Au$_n$Mn isomers tend to occupy the most highly coordinated position. Wang *et al.*[17] investigated 2D to 3D structural transitions in gold cluster anions, due to isoelectronic substitution of a single Ag or Cu atom in Au$_N$, for $N = 8 - 11$. Later on Pal *et al.*[18] extended this pursuit to Au$_n$ anions with $N = 12 - 14$, also doped with a single Ag or Cu atom. Heiles *et al.*[12] studied Au$_n$Ag$_{8-n}$ over the whole composition range, by means of a genetic algorithm coupled with density functional theory calculations. It is interesting to notice that they obtained basically only two distinct conformations, one planar and one fully 3D, for all the putative ground states over the whole range of compositions. Hong *et al.*[19] investigated Au$_m$Ag$_n$ ($5 \le m+n \le 12$) binary clusters, using a genetic algorithm search in combination with first-principle calculations. They analyzed the effects of size and composition, and established the critical gold silver ratios for the 2D↔3D transition. Their ground state conformations for Au remained planar up to their maximum of 12, while Ag clusters adopted 3D structures for $N \ge 7$. Tafoughalt and Samah[20] performed a detailed DFT study of the Au$_n$Ag$_{8-n}$ system, and more recently[9] also of the AgAu$_{N-1}$ system for $3 \le N \le 13$. Kuang *et al.*[21] carried out an all-electron scalar relativistic calculation of Au$_N$Ag ($N = 1 - 12$) clusters, which limited its scope to the doping of the Au cluster with a single Ag atom. Recently Barron *et al.*[10]

^{a}Departamento de Física, Facultad de Ciencias, Universidad de Chile, Casilla 653, Santiago, Chile 7800024

^{b} Centro para el Desarrollo de la Nanociencia y la Nanotecnología (CEDENNA), Avda. Ecuador 3493, Santiago, Chile 9170124

^{c} Nano-Bio Spectroscopy Group and ETSF Scientific Development Centre, Departamento de Física de Materiales, Universidad del País Vasco UPV/EHU, Av. Tolosa 72, E-20018 San Sebastián, Spain

*E-mail: m.kiwi.t@gmail.com

using DFT computed both the structural and electronic properties of 13-atom AgAu nanoalloys, but limited their interest to 3D configurations.

Here we report on the structural and electronic properties of the putative ground states, and low lying excited states, for all possible n values, of $Au_{13-n}Ag_n$ clusters. We compute the binding energy, the energies of the ground state and of the first two excited conformations, and their corresponding electronic structure. We conclude that only few essentially different types of geometries are relevant to describe all the low lying energy conformations of these clusters.

2 Method

To obtain the groundstate conformation of a binary nanocluster is a rather formidable task. In fact, on the basis of a Lennard-Jones potential, Wales and Doye[22] estimated the number of local minima of a pristine 55 atom cluster to be $\sim 10^{21}$, while Rogan et al.[1] estimated it at $\sim 10^{22}$. However, when different species are combined, in order to create an alloy cluster, the number of different atomic arrangements that the cluster can adopt increases very significantly because of the many ways the atoms can be spatially distributed.[1]

If the problem of finding the groundstate of a pure cluster with more than ~ 7 atoms is a truly challenging problem, and constitutes an open topic of current research;[1,22–25] the problem of dilute alloys (i.e. very low concentration of one of the atomic species) is way harder, since there is an extra degree of freedom: all the different species permutations that are consistent with a given geometry (homotops). For nanoclusters the number of homotops increases as the combinatorial of the total number of atoms (in our case $N = 13$) and the particular element, namely $N!/(n!(N-n)!)$ with $1 < n < N$, which makes the computations extremely demanding. Consequently, the exploration of all the local minima becomes a prohibitive effort, and alternative approaches have to be implemented.

We employed a diversity-based approach, that is, we divided the problem into two parts: i) the generation of a structure bank of different putative minimal energy nanocluster structures; and ii) a DFT search for the putative groundstate, and the conformations of low lying energies. Since our findings do not completely agree with some previous work, an extensive search is well justified and particularly important. The full details of our search strategy can be found in Appendix 4.1.

To generate the structure banks we employed a classical potential. However, we generated both 3D and 2D conformations. To obtain the latter we added geometrical constraints to force the generation of planar seeds. To insure diversity within the structure bank we used the distance between different clusters, as formulated by Grigoryan et al.,[26,27] as an additional criterion.

A rough ab-initio optimization was applied to each seed in the structure bank (about 1.000 seeds for each stoichiometry), followed by an accurate DFT optimization (detailed in Appendix 4.2), that was performed on 30 selected seeds and several of their homotops (again, for each stoichiometry). For the all the DFT computations the VASP package was employed. We performed this latter optimization using the TPSS[28] metaGGA and PBE[29] functionals for the exchange-correlation term (XC). The PBE functional has been extensively employed in studies of coinage metal clusters, due to its simplicity and its degree of success when compared to experiments.[17,18,30] However, PBE suffers from several drawbacks, like overestimating the stability of neutral 2D Au clusters; in fact, it predicts a planar groundstate for Au_{13} clusters. In contrast, the TPSS functional is known to yield accurate results. For instance, according to Götz et al.[11] the error in the evaluation of the Au dimer bond length, as compared with experimental data, is $\sim 0.8\%$ for TPSS, while it is $\sim 2.1\%$ for PBE. Götze found that the performance of this functional was very close to the wavefunction-method coupled cluster singles, doubles plus perturbative triples [CCSD(T)], giving the correct ordering of the different isomers. Similarly, Johansson et al.[8] found a very good performance of TPSS, compared to RPA (random-phase approximation). An extra bonus is that the use of the two functionals allows to compare the extent to which the results depend on the XC that is implemented.

3 Results

3.1 2D and 3D energetics

The binding energies of the most stable 2D and 3D structures, obtained by means of the procedure described above, are illustrated in Fig. 1. The transition from 2D to 3D for the $Au_{13-n}Ag_n$ clusters depends on the exchange correlation functional employed and on relativistic effects. Without spin-orbit coupling (SOC) the transition occurs at $n = 1$ for TPSS and at $n = 2$ for PBE. Consequently, only the Au_{13} groundstate should be planar for TPSS, while $Au_{12}Ag$ should still be planar for PBE. But when the SOC interaction is included there is a clear tendency towards a 3D groundstate, and there is no planar groundstate for TPSS, while for PBE only the pristine Au_{13} cluster remains planar. However the energy difference between the 2D and 3D groundstates (ΔE_b) is quite small for small n. For $n = 0, 1$ (TPSS), and for $0 \leq n \leq 3$ (PBE) ΔE_b/atom is smaller than the equivalent room temperature.

The behavior of the energy difference between both structures, ΔE_b, is quite independent of the XC functional, and for small n it increases almost monotonically, but it is steeper for TPSS. Thus ΔE_b reaches a maximum value at $n = 9$ where it

stabilizes. Wang *et al.*[17] experimentally found that in anionic gold clusters a single Ag impurity shifts the 2D-3D transition to a smaller size. Heiles *et al.*,[12] when studying 8-atom Ag-Au clusters, also found the transition for $n = 2$, however the total energy differences between the various concentrations they reported are much larger ($0.05 - 0.10$ eV), and despite of the fact that they did not included SOC, their results are trustworthy. Therefore, 2D clusters are -in principle- likely to be found in experiments for low Ag concentrations, but other effects may hinder their occurrence.[31] It is worth remarking that for neutral clusters the expected 2D-3D crossover is predicted, by RPA and TPSS calculations,[8] to occur for Au_{11}.

Both panels of Fig. 1 show an interesting behavior, the curves are almost 'degenerate' for $n = 0$ and $n = 13$. None of these apparent crossings are accidental: for $n = 0$ the 2D and 3D conformations have almost the same energy, while SOC largely increases the stability of the 2D and 3D clusters. For $n = 13$ it is the opposite; the energy difference between 2D and 3D cluster is quite large, but the SOC is small for pure Ag clusters. Finally, there is a crossing at an intermediate region, which does not have a trivial physical explanation, but it is interesting that it happens at the transition from a mostly Au to a mostly Ag motif, as is apparent when crossing from the yellow to the light blue regions of Fig. 1.

3.2 Low energy conformations

A recurrent topic in the search of low energy cluster conformations is the lack of trends. However, in the case at hand the groundstate and their first higher energy isomer are remarkable simple, regardless of the sophistication of the XC functional employed, as illustrated in Fig. 2. It is quite apparent that all the planar low lying conformations are quite similar (and also for planar isomers in TPSS that are not shown), which is plausible because of the limited available conformational space for the 2D configurations, as compared with the 3D arrangements.

Moreover, while there is a huge number of possible 3D configurations, their groundstate conformations are few. In fact, most 3D groundstates adopt just two different conformations, and the lowest energy isomers are likely to be homotops of the groundstate. The Au_{13} (TPSS) geometry (see Fig. 2 for the labeling) or a slightly deformed version, correspond to the groundstates adopted by $Au_{12}Ag$ to Au_5Ag_8 for TPSS, and up to Au_6Ag_9 for PBE. Similarly, the geometry of Au_6Ag_7 (TPSS) corresponds to the minimum energy of the conformations adopted by clusters up to Au_2Ag_{11} for both functionals.

It turns out that only in two cases the two functionals yield important differences: i) for the pure and dilute Au-rich (Au_{13}, $Au_{12}Ag$) and Ag-rich (Ag_{13}, $AuAg_{12}$) clusters, and ii) for the transition between geometrically different motifs (Au_5Ag_8 to Au_6Ag_7). However, in the latter case only two geometries,
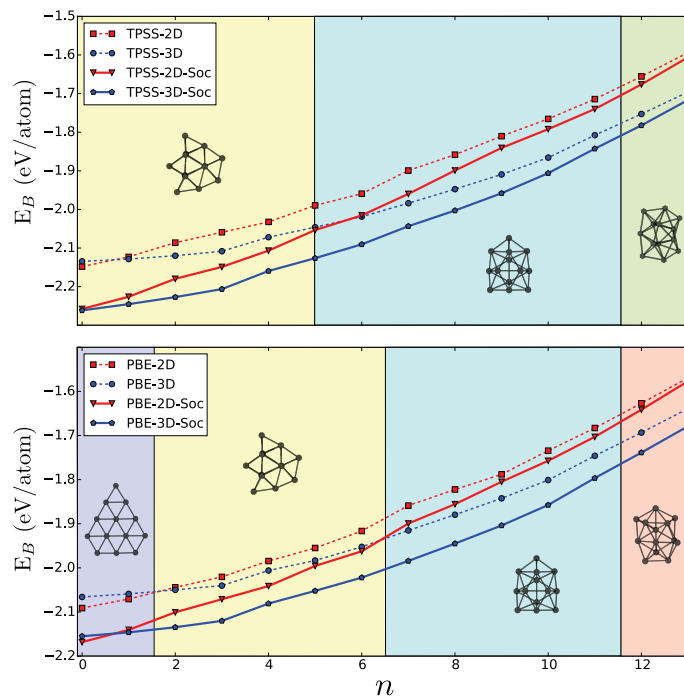
Fig. 1 Binding energy (E_B) of the most stable 2D and 3D $Au_{13-n}Ag_n$ cluster for each concentration n. The upper (lower) panel corresponds to the calculation with the TPSS (PBE) exchange correlation functional. The continuous (dashed) lines are the results with (without) including spin-orbit coupling (SOC). The conformations that are illustrated correspond to the lowest energy ones in the different regions (n values). Additional details are given in Fig. 3.

and their deformations, are of interest.

Homotops of quite similar geometries populate the low-lying energies. This means that -roughly speaking- two energy scales are present; one determined by the geometry itself (the motif), and one due to the homotops. While the former energy scale can have total energy differences that range from zero to a few eV, the latter energy range is usually less than 0.1 eV. Such a behavior is apparent by inspection of Fig. 2 where more than two atoms of any of the elements are present; *i.e.* when the homotops are more important, the total energy difference between the groundstate and the first isomer is less than 0.05 eV. Therefore, at least in our case, the search for low-energy clusters can be decoupled into a search of geometries followed by a 'fine-tuning' of the atomic arrangements. However, the behavior of the two functionals yields different results: while for PBE both energy scales are well-separated (*i.e:* the actual decoration is not very important), for TPSS they are closer and often mixed. Therefore, it is worth building carefully the seed structure bank, to avoid 'false negative' results due to under-sampling. To validate our results we briefly compare them with the literature. Johansson *et al.*[8] studied

Fig. 2 Most stable configurations, using the TPSS and PBE exchange correlation. The number below each conformation is the energy difference (in eV) relative to the respective groundstate in each row (fixed n). Yellow (gray) spheres label Au (Ag) atoms.

neutral Au clusters of up to 13 atoms, using TPSS and other methods, and we obtain the same putative groundstate and the first higher energy isomer.

Several authors have studied theoretically pure Ag_{13} clusters. Baishya et al.[30] found all the structures reported here, but with a different energy ordering. Jin et al.[32] studied the neutral, cationic, and anionic cases, and their results are similar to ours (at the PBE level). Surprisingly, their minimal energy structure of Ag_{13}^- coincides with the neutral Au-rich motif of our study. Harb et al.[33] showed that the optical absorption spectra (experimental) of neutral Ag_{13} corresponds to the same geometry that we report here. Yong et al.[7] reported a cage-like Ag_7Au_6 which bears similarities with, but is different to the structure that we propose. In fact, our motif is not among their low-lying isomers. They used a structural search based on the replacement of atoms of pure clusters, suggesting the need to have a fairly diverse structure bank, as the one we constructed here.

Kuang et al.[21] found a planar groundstate for Au_{13} and $Au_{12}Ag$, using the Perdew-Wang functional, which overestimates the stability of planar clusters much like PBE. Our result using PBE thus agrees with theirs. Tafoughlat and Samah[20] studied dilute $AgAu_n$ clusters using the Wu-Cohen functional. They found a 3D $Au_{12}Ag$ cluster that resembles our groundstate. Barron et al.[10] studied the complete series of 13 atom AuAg clusters. However, they limited their attention to a few motifs to obtain the minimum energy conformation, and concluded that for this size clusters there is no segregation, a conclusion that agrees with the structures we report. Hong et al.[19] studied AuAg nanoclusters of up to 12 atoms. They employed PBE, and therefore their results are biased towards 2D motifs for Au-rich clusters. While smaller, their structures strongly resemble the motifs we obtained with PBE. Also, they found a simple trend of two different geometries, and that the low energy isomers are mostly due to the different homotops.

In a seminal paper Chen and Jonhston[34] studied 13 atom AuAg clusters, using a genetic algorithm in combination with the Gupta potential. Due to the use of a classical potential they found mostly icosahedral structures, which lie far above in energy from most bi-planar structures.[10] To be fair the Chen and Jonhston results were published in 2007, and a DFT optimization involving that many structures was prohibitive at that time.

3.3 Electronic Structure

We now focus our attention on the electronic structure of the configurations we obtained. Fig. 3 shows the Kohn-Sham energy eigenvalues for fixed 2D and 3D geometries, for all possible compositions (n values) of Au_nAg_{13-n}. The aim of this figure is to explain qualitatively some of the trends already found, but neglecting the differences among homotops (we
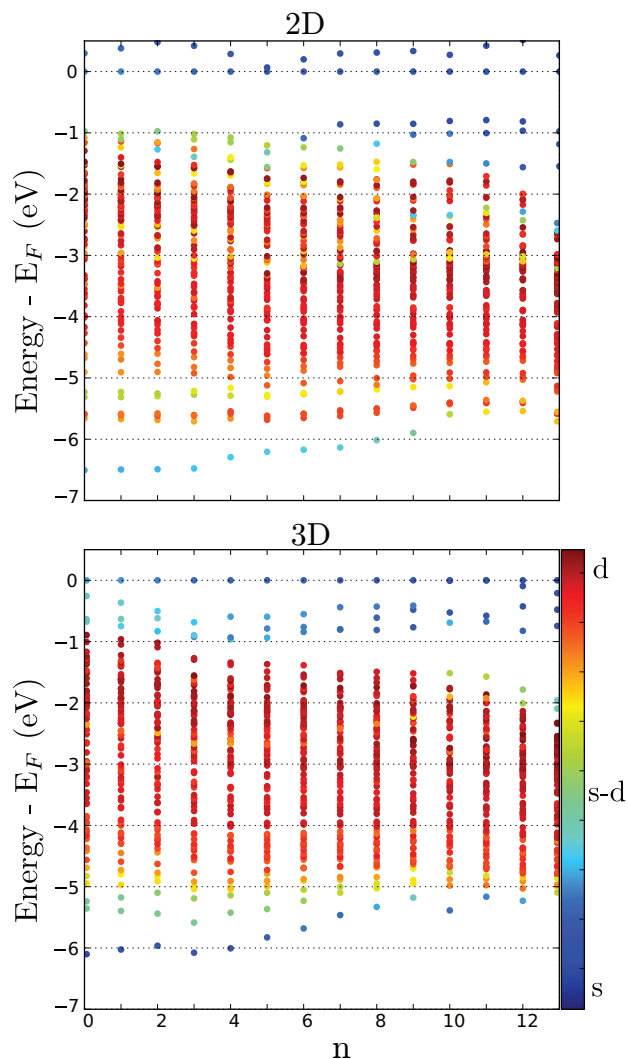
Fig. 3 Energy levels of 2D (upper panel) and 3D (lower panel) $Au_{13-n}Ag_n$ clusters as a function of the number n of Ag atoms. The darker the red (blue) the stronger the d (s) character. All the energies are relative to E_F, the HOMO/LUMO energy, since the HOMO and LUMO levels are degenerate. The clusters are generated from the two first geometries of the lower panel Fig. 1. The effects due to the homotops are discussed later on.

will return to this point at the end of this section). The energy levels correspond to PBE calculations, which coincide qualitatively with the TPSS functional results.

Since gold is non-magnetic and there is an odd number of atoms, the HOMO and LUMO for all concentrations are degenerate, and we choose it as the $E = 0$ level. For both 2D and 3D structures, and for most concentrations, the lowest energy levels are s-like, followed by a large region of d-like levels, as illustrated in Fig. 3. But 2D clusters display a large hybridization of the lowest energy level with the d levels (actu-

ally with dz^2). This sd character is due to relativistic effects on the 6s states.[6] These 'free electron' 6s-5d states are shifted from above to below the 5d band. In fact, this is the behavior found in bulk Au and weakens as the Ag concentration increases, where these states are found mostly above the 5d band.

An interesting feature is that the 5d band becomes broader as the Au concentration increases. This is also due to a relativistic effect that removes the degeneracy of the d-orbitals. The main effect of the spin-orbit coupling, when included, is to enhance this splitting even further for a heavy element like Au. Another interesting behavior of the 3D clusters is that this lowest energy level increases its energy as the number of Ag atoms grows from 4-5 to 8-9 (see Fig. 3).

Finally one may ask about the impact that the various homotops have on the electronic structure. Fig. 4 shows the energy levels for two extreme cases, a mostly Au and a mostly Ag cluster, but when both clusters have the same geometry. It is evident that the electronic structure is quite insensitive to the atomic arrangement. However, changing the atomic species (i.e.: the concentration) yields large energy level shifts. Also, it is worth noticing that all these features (like the shift of the 5s band) are also present for the rest of the clusters we studied.

4   Conclusions

In this contribution we calculated structural and electronic properties of $Au_{13-n}Ag_n$ for all values of n, focusing our interest on the 2D↔3D crossover. We start creating a structure bank of minima by means of phenomenological potentials, which were refined by means of DFT. An additional homotop enrichment was generated using $n-1$ and $n+1$ low lying energy structures, in order to reduce the bias in the search for optimal low energy conformations. This way we obtained the putative ground state conformations, and those of the low lying excited states, as well as the energies of their electronic states.

We found that, using the TPSS functional with spin-orbit coupling, the whole series does not have planar ground-states. Without spin-orbit, only the Au_{13} groundstate is planar. For the PBE exchange-correlation term up to the Au_{13} and Au_1Ag_{12} groundstate are planar, with and without spin-orbit coupling. However, despite the fact that no planar conformations were found with TPSS+SOC, planar isomers up to Au_1Ag_{12} are energetically competitive (*i.e.:* the energy difference is smaller than room temperature).

Using TPSS, almost all the relevant conformations of the alloyed clusters belong to just two variants, which are a Au-rich phase up to $n = 5$, and a Ag-rich phase for $n \geq 6$. This is largely independent of the XC functional employed. Conversely, for the pure and dilute cases no trends are apparent,
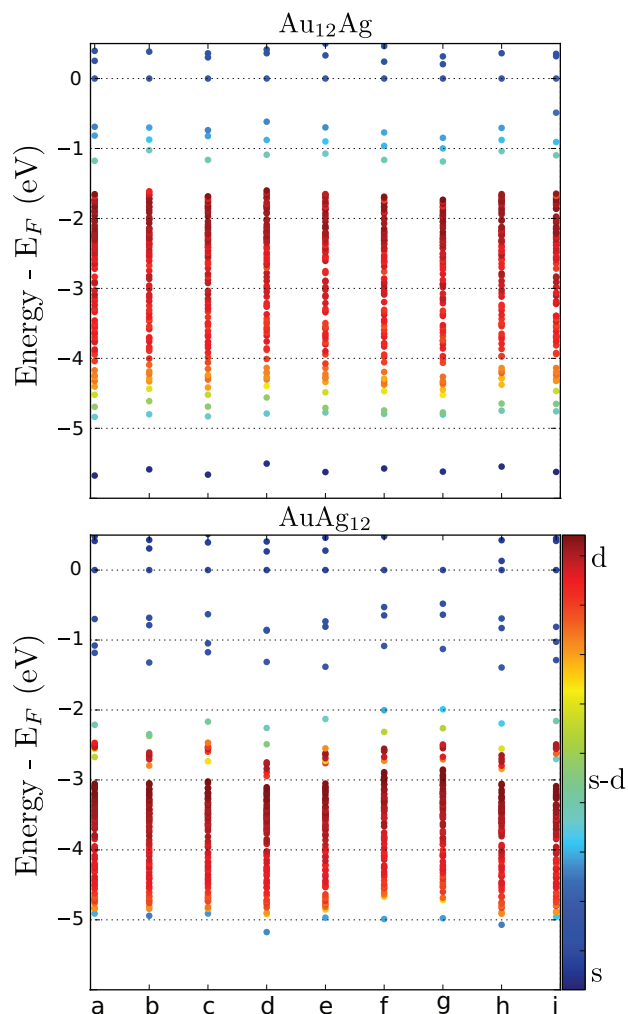
Fig. 4 Energy levels of $Au_{12}Ag$ and $AuAg_{12}$ clusters for all their nonequivalent homotops (labeled a-i). The color scale indicates its character, reddish (bluish) correspond to d (s). All the values are respect to the HOMO/LUMO energy, E_F. The selected geometry, based on which we construct the homotops, corresponds to the Au_6Ag_7 groundstate that is illustrated in Fig. 2.

and the results of different functionals are in disagreement.

For most concentrations of the 2D and 3D structures the lowest energy levels are s-like, followed by a large region of d-like levels. However, for the 2D conformations there is a large hybridization of the lowest energy level with the dz^2 states, due to relativistic effects on the 6s states. As the number of Ag atoms grows the 5d band narrows (a relativistic effect), and when the number of Ag atoms increases from ~ 4 to ~ 9 the energy of this level becomes larger.

Appendix: Methods

4.1 Structure Bank generation

The structure bank of nanocluster conformations was generated using the procedure developed by Rogan et al.[1], with the semi-empirical Gupta potential.[2,3] It is well-known that these classical potentials fail to agree with DFT calculations, especially for 2D clusters.[35] To overcome this problem we generated two independent structure banks for each Ag concentration (n value) by optimizing 10^7 random structures, using the strategy developed by Rogan et al.[1] The first structure bank is constrained to include only planar conformations (i.e. only 2D structures), while on the second one no constraints are imposed, thus allowing for 3D clusters.

After this minimization process, we keep only the conformations that are truly different, by sorting the minimized configurations according to their energies, and discarding the ones with the same energy. Next, we select ~ 1000 planar configurations, and ~ 9000 volumetric ones, maximizing the structural differences between each one of the 1000 (9000) configurations of the 2D (3D) structure bank. In order to do so we use the Grigoryan et al. distance criterion,[26,27] which defines two N atom clusters, A and B, as the same if

$$D_{A,B} = \left(\frac{2}{N(N-1)} \sum_{i=1}^{N(N-1)/2} \left(d_i^{(A)} - d_i^{(B)} \right)^2 \right)^{1/2} = 0 \, , \quad (1)$$

where $d_i^{(A)}$ is the sorted list of $N(N-1)/2$ interatomic pair distances of each cluster, without distinction of species. This measure has the significant advantage of being translationally and rotationally invariant.

By constraining the distance $D_{A,B}$ between any couple of clusters A and B to be larger than a certain critical value D_c, which depends on the set of structures in each structure bank, we limit the number of structures in each bank to reach ~ 1000 planar, and ~ 9000 three dimensional ones. At the same time we maximize the structural difference between them, reducing the possibility that many configurations converge to the same final structure in the subsequent DFT calculations.

The phenomenological Gupta potential is adjusted to fit the cohesion energy of a particular *bulk* material.[3] It is based on the tight binding second moment approximation[36] and has two terms. An attractive many-body part

Table 1 Parameters corresponding to the homonuclear Ag-Ag, and Au-Au interactions on the Gupta potential.

Interaction	A (eV)	ξ (eV)	p	q	r^0 (Å)
Ag-Ag	0.1028	1.178	10.928	3.139	2.889
Au-Au	0.2061	1.790	10.229	4.036	2.884

$$E_{\mathrm{mb}}^i = \left(\sum_{j \neq i} \xi_{(a,b)}^2 \exp \left\{ -2q_{(a,b)} \left(\frac{r_{ij}}{r_{(a,b)}^0} - 1 \right) \right\} \right)^{1/2}, \quad (2)$$

and a repulsive Born-Mayer type repulsion, which insures stability, and is given by

$$E_{\mathrm{r}}^i = A_{(a,b)} \sum_{j \neq i} \exp \left(-p_{(a,b)} \left(\frac{r_{ij}}{r_{(a,b)}^0} - 1 \right) \right). \quad (3)$$

Here a and b label the elements; r_{ij} is the distance between atoms i and j; r^0 is the nearest neighbor bulk interatomic distance; and A, ξ, p, and q are the parameters that are fitted to bulk properties, namely the cohesive energy, the bulk modulus, and the vanishing of the energy gradient at r^0, respectively.

Finally, the system cohesive energy is given by

$$E_{\mathrm{c}} = \sum_i (E_{\mathrm{r}}^i - E_{\mathrm{mb}}^i). \quad (4)$$

The parameters corresponding to the homonuclear Ag-Ag, and Au-Au,[2] interactions are summarized in Table 1. The parameters for the heterogeneous Au-Ag interaction were constructed as the geometric mean of the respective homonuclear parameters.

4.2 DFT optimization

The DFT optimization was performed using the VASP package,[37–39] PAW-type pseudopotentials,[40] and the so-called PBE exchange-correlation.[29] All the $\sim$10000 above mentioned selected seeds (2D and 3D), were optimized until each atomic force became smaller than 0.05 eV/Å. An energy cutoff of 200 eV was employed, which is sufficient to obtain a rough estimate of the energy ordering for the seed geometries, while keeping the computing time within reasonable limits.

Next, for each Ag concentration n of the $Au_{13-n}Ag_n$ system, the 10 lowest energy geometries for $n-1, n, n+1$ (30 in total) were selected as seeds for further exploration of the different geometries; that is, a Ag atom was exchanged for a Au one from the $n-1$ structure bank of low energy conformations, to be employed as a seed. The inverse exchange was carried out for the $n+1$ structure bank. Up to 30 homotops were generated for each of the previous structures, that is

about 900 different clusters for every n value. Since now the energy difference between the many structures can be quite small, we employed a larger cutoff (250 eV), and a tighter convergence criterion on the forces (0.01 eV/Å). Due to the shortcomings of PBE, at this step we also used the TPSS metaGGA functional,[28] which is recognized for its accuracy to describe Au nanoparticles. Finally we turn-on the spin-orbit coupling, since it is sizable for Au, as implemented by Koelling and Harmon.[41]

References

1 J. Rogan, A. Varas, J. A. Valdivia and M. Kiwi, *J. Comput. Chem.*, 2013, **34**, 2548–2556.

2 F. Cleri and V. Rosato, *Phys. Rev. B*, 1993, **48**, 22–33.

3 R. P. Gupta, *Phys. Rev. B*, 1981, **23**, 6265–6270.

4 L. Xiao and L. Wang, *Chem. Phys. Lett.*, 2004, **392**, 452 – 455.

5 B. Yoon, P. Koskinen, B. Huber, O. Kostko, B. von Issendorff, H. Häkkinen, M. Moseler and U. Landman, *Chem. Phys. Chem.*, 2007, **8**, 157–161.

6 H. Hakkinen, *Chem. Soc. Rev.*, 2008, **37**, 1847–1859.

7 Y. Yong, C. Li, X. Li, T. Li, H. Cui and S. Lv, *J. Phys. Chem. C*, 2015, **119**, 7534–7540.

8 M. P. Johansson, I. Warnke, A. Le and F. Furche, *J. Phys. Chem. C*, 2014, **118**, 29370–29377.

9 M. Tafoughalt and M. Samah, *Comput. Theor. Chem.*, 2014, **1033**, 23 – 30.

10 H. Barron, L. Fernandez-Seivane, H.-C. Weissker and X. Lopez-Lozano, *J. Phys. Chem. C*, 2013, **117**, 21450–21459.

11 D. A. Götz, R. Schäfer and P. Schwerdtfeger, *J. Comput. Chem.*, 2013, **34**, 1975–1981.

12 S. Heiles, A. J. Logsdail, R. Schafer and R. L. Johnston, *Nanoscale*, 2012, **4**, 1109–1115.

13 M. Haruta, *Catal. Today*, 1997, **36**, 153 – 166.

14 X. Huang, I. H. El-Sayed, W. Qian and M. A. El-Sayed, *J. Am. Chem. Soc.*, 2006, **128**, 2115–2120.

15 D. Wu, X.-D. Zhang, P.-X. Liu, L.-A. Zhang, F.-Y. Fan and M.-L. Guo, *Curr. Nanosci.*, 2011, **7**, 110–118.

16 D. Dong, K. Xiao-Yu, G. Jian-Jun and Z. Ben-Xia, *J. Phys. Chem. Solids*, 2010, **71**, 770 – 775.

17 L.-M. Wang, R. Pal, W. Huang, X. C. Zeng and L.-S. Wang, *J. Chem. Phys.*, 2010, **132**, 114306.

18 R. Pal, L.-M. Wang, W. Huang, L.-S. Wang and X. C. Zeng, *J. Chem. Phys.*, 2011, **134**, 054306.

19 L. Hong, H. Wang, J. Cheng, X. Huang, L. Sai and J. Zhao, *Comput. Theor. Chem.*, 2012, **993**, 36 – 44.

20 M. Tafoughalt and M. Samah, *Physica B*, 2012, **407**, 2014 – 2024.

21 X.-J. Kuang, X.-Q. Wang and G.-B. Liu, *J. Alloys Comp.*, 2013, **570**, 46 – 56.

22 D. J. Wales and J. P. K. Doye, *J. Phys. Chem. A*, 1997, **101**, 5111–5116.

23 C. J. Tsai and K. D. Jordan, *J. Phys. Chem.*, 1993, **97**, 11227–11237.

24 D. J. Wales and H. A. Scheraga, *Science*, 1999, **285**, 1368–1372.

25 J. P. K. Doye, M. A. Miller and D. J. Wales, *The Journal of Chemical Physics*, 1999, **111**, 8417–8428.

26 V. G. Grigoryan and M. Springborg, *Chemical Physics Letters*, 2003, **375**, 219 – 226.

27 V. Grigoryan, D. Alamanova and M. Springborg, *The European Physical Journal D-Atomic, Molecular, Optical and Plasma Physics*, 2005, **34**, 187–190.

28 J. Tao, J. P. Perdew, V. N. Staroverov and G. E. Scuseria, *Phys. Rev. Lett.*, 2003, **91**, 146401.

29 J. P. Perdew, K. Burke and M. Ernzerhof, *Phys. Rev. Lett.*, 1996, **77**, 3865.

30 K. Baishya, J. C. Idrobo, S. Öğut, M. Yang, K. Jackson and J. Jellinek, *Phys. Rev. B*, 2008, **78**, 075439.

31 P. Koskinen, H. Häkkinen, B. Huber, B. von Issendorff and M. Moseler, *Phys. Rev. Lett.*, 2007, **98**, 015701.

32 Y. Jin, Y. Tian, X. Kuang, C. Zhang, C. Lu, J. Wang, J. Lv, L. Ding and M. Ju, *J. Phys. Chem. A*, 2015, **119**, 6738–6745.

33 M. Harb, F. Rabilloud, D. Simon, A. Rydlo, S. Lecoultre, F. Conus, V. Rodrigues and C. Felix, *J. Chem. Phys.*, 2008, **129**, 194108.

34 F. Y. Chen and R. L. Johnston, *Appl. Phys. Lett.*, 2007, **90**, 153123.

35 M. Munoz, A. Varas, C. Cardenas, J. Rogan and P. Fuentealba, *Comput. Theor. Chem.*, 2013, **1021**, 249 – 255.

36 J. C. Slater and G. F. Koster, *Phys. Rev.*, 1954, **94**, 1498–1524.

37 G. Kresse and J. Hafner, *Phys. Rev. B*, 1993, **47**, 558.

38 G. Kresse and J. Furthmüller, *Comput. Mat. Sci.*, 1996, **6**, 15.

39 G. Kresse and J. Furthmüller, *Phys. Rev. B*, 1996, **54**, 11169.

40 G. Kresse and D. Joubert, *Phys. Rev. B*, 1999, **59**, 1758.

41 D. D. Koelling and B. N. Harmon, *J. Phys. C*, 1977, **10**, 3107.